DETERMINATION OF THE LONGITUDINAL COMPRESSIVE STRENGTH OF UD PLIES CONSIDERING DIFFERENT CLASSICAL AND INNOVATIVE TESTS

F. Laurin[1*], A. Mavel[1], P. Paulmier[1] and F.-X. Irisarri[1]

[1] ONERA, Paris Saclay-University, Châtillon, France, frederic.laurin@onera.fr

Keywords: Longitudinal compressive strength, Multi-instrumented tests, multiscale analysis modelling, design allowable

ABSTRACT

The present study has proposed a critical analysis of the available existing tests in order to determine the longitudinal compressive strength of a UD ply. The (i) standardized compressive tests on UD-ply, the (ii) alternative tensile test on a specific lay-up proposed by ONERA and (iii) additional bending tests on UD-ply have been considered. The measured compressive strength at the ply scale is different for those tests and the highest strength value is obtained for bending loadings. In order to analyze such tests (compression, tension and bending), a micromechanical model, associated to a ply scale damage model, has been considered and allows demonstrating that the variation of the longitudinal compressive strength obtained at the UD ply scale for tension and bending tests are consistent if fiber kinking is considered at microscale scale, which seems to be the relevant scale of analysis.

1 INTRODUCTION

Composite materials and especially carbon fibre reinforced plastics (CFRP) are widely used in modern aircrafts. Currently, the design methods of laminated composite structures mainly rely on linear elastic structural analysis combined with failure criteria [1] defined at the scale of the elementary unidirectional (UD) ply. Thus, determining the design allowable, *i.e.* the ply strengths taking into account material scattering as recommended in the aeronautical standards [2], is a major concern for the designers. Indeed, determination of the design allowable is a time consuming and expensive process, since a large number of tests are required. In order to reduce cost and product lead-time, fast and simple identification tests and analysis methods are required. Moreover, proposing identification tests with low coefficients of variation (CV) will increase the A- and B-basis allowable [2], resulting in higher performance designs. Among the in-plane strengths of a unidirectional ply, the determination of the ply longitudinal compressive strength currently remains a technical and scientific challenge.
This article analyses different existing tests to determine the longitudinal compressive strength of a unidirectional ply, from classical compressive tests, considering also bending tests, to innovative tensile on a specific laminate in section 2. A failure approach, considering the unidirectional ply as the elementary modelling entity but some material parameters are updated thanks to the use of a micromechanical model, has been developed to predict fibre kinking in composite laminates subjected to different loadings, as presented in section 3.

2 TESTS TO DETERMINE THE LONGITUDINAL COMPRESSIVE STRENGTH

In this section, the determination of the longitudinal compressive strength of carbon/epoxy T700GC/M21 unidirectional plies, with a weight areal of 268g/m^2, has been performed considering different classical and innovative tests. All the composite specimens have been manufactured at ONERA considering a hot press and the curing cycle corresponds to that recommended by the material provider.

2.1 Standardized compression test on UD plies

The longitudinal compressive strength, associated with the onset of fibre kinking, could usually be identified using some standards considering uniaxial compressive tests on unidirectional 0° laminates [3,4]. However, this kind of test is very difficult to perform in order to obtain reliable and reproducible

results. Indeed, the design of compressive tests on 0° laminates necessitates considering carefully two major aspects: (i) the introduction of the applied loading and (ii) the geometry of the specimens.
In this study, standard compression tests on 16-ply 0°-laminates have been performed at ONERA according to the EN2850 AECMA standard [5]. The total thickness of the plate is about 4.20 mm. 18 specimens have been machined. Compressive force is transmitted into the specimen through end-loading, thus avoiding the use of additional tabs. The compressive tests have been conducted by means of an electro-mechanical Schenck machine of 150 kN maximum capacity, illustrated in Figure 1a. The tests are controlled in displacement with a 0.1 mm/min constant displacement rate. For all compression tests, digital image stereo-correlation and acoustic emission have been used.

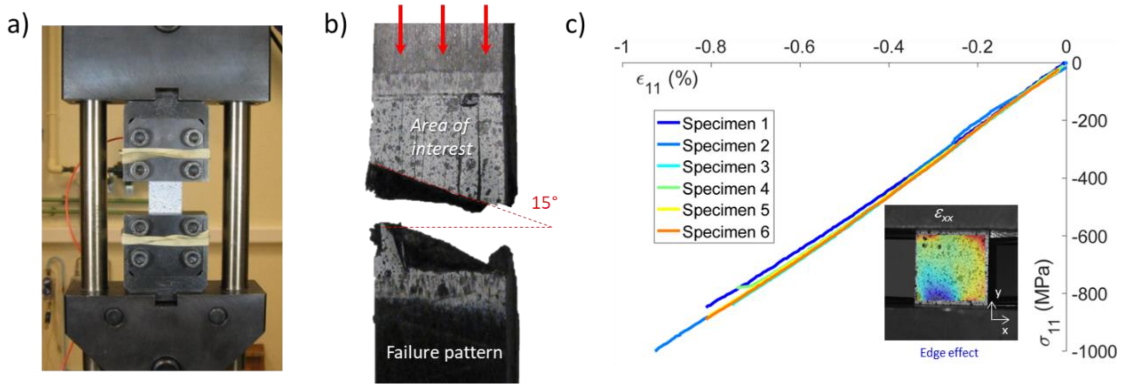

Figure 1 : a) Experimental device at ONERA, b) Failure pattern on 0-ply compression test and c) measured stress/strain curves at failure

A special attention has been paid to the parallelism of the loaded faces and to their roughness. In accordance with the EN2850 AECMA standard [5], six specimens have a 10 mm side square gauge area. These specimens are called “standard” in the following. Figure 1c shows the macroscopic stress / strain curves of the specimens up to failure. The longitudinal strain is evaluated using a virtual strain gauge located in the centre of the gauge section with a grid size of 7 mm x 7 mm. The average measured fibre compressive strength is X_c = -880 MPa with 9.9 % CV. Failure of the specimens occurs close to the test machine grips as shown in Figure 1b. This failure mode is typical of this kind of test and explains both the low average strength value and the large scattering of the experimental data at failure.
In order to quantify the influence of the specimen size on the identified strength, as reported by Lee and Soutis [4], additional compression tests have been performed on larger samples. “Type A” specimens have a 10 mm gauge length and a 25 mm gauge width. “Type B” specimens have a 25 mm side square gauge area. For each configuration, six specimens have been tested up to failure. The experimental stresses and strains at failure are given in Table 1.

Specimens	Gauge area mm x mm	Stress at failure MPa (CV %)	Strain at failure % (CV %)
standard	10 x 10	-880 (9.8)	-0.80 (10.8)
Type A	25 x 10	-920 (5.9)	-0.82 (12.7)
Type B	25 x 25	-924 (4.2)	-0.86 (5.7)

Table 1: Geometry, stress and strain at failure for the 3 configurations of compressive tests on 0-plies

As observed by Lee and Soutis [4], the average value of X_c increases significantly with the size of the specimens while scattering decreases, larger specimens being less sensitive to edge effects. However, failure still occurs close to the test grips. The standard compression tests on 0-specimens are affected by edge effects and the multi-axial stress states under the test grips that trigger premature failure and large scattering of the test results, whereas the proposed tensile test is free of such drawbacks. Note that, for all configurations, strain at failure in the longitudinal direction, $X_{\varepsilon c}$, is a direct result of the test.

2.2 Bending tests on UD plies

Several authors proposed to use bending tests to circumvent the difficulties inherent to compression testing of unidirectional laminates. Indeed, for a carbon/epoxy unidirectional ply, the longitudinal compressive strength is much lower than the longitudinal tensile strength. Thus, three-point bending tests [6,7] and four-point bending tests [8] are relevant to identify the compressive strength in the fibre direction. However, both test set-ups generate high stress concentrations under the rollers which can lead to local indentation and premature failure of the specimen. The compression with pivots testing device [9] allows to generate bending loading by off-setting the mid-plane of the laminate with respect to the rotation axes of the pivots, as an alternative to the existing bending testing devices previously developed [10–14]. This device allows to avoid both local stress concentrations close to the jaws and roller indentation issues experienced with the aforementioned testing set-ups. Moreover, it enables direct observation of the compressive failure on the surface plies of the laminate. Due to the use of a bending loading mode, the failure mechanism is observed in the gauge section, far from the jaws.
Therefore, Figure 2a presents an original experimental device of compression with pivots. The idea consists in applying a uniform compression to a laminate plate clamped in two jaws with pivots. The eccentricity of a given test relates to the offset of the mid-surface of the plate, imposes the ratio of compression versus bending. It is controlled through the use of a couple of wedges that are inserted adequately in the jaws of the tabs. For a large eccentricity, the specimen is subjected to a quasi-pure bending moment (as encountered with the four-point-bending test device), while for small eccentricity the test tends to a pure compression test. In the present study, large eccentricities, equal to half of the total thickness of the tested specimen, are used in order to obtain quasi-pure bending moment in the gauge length.

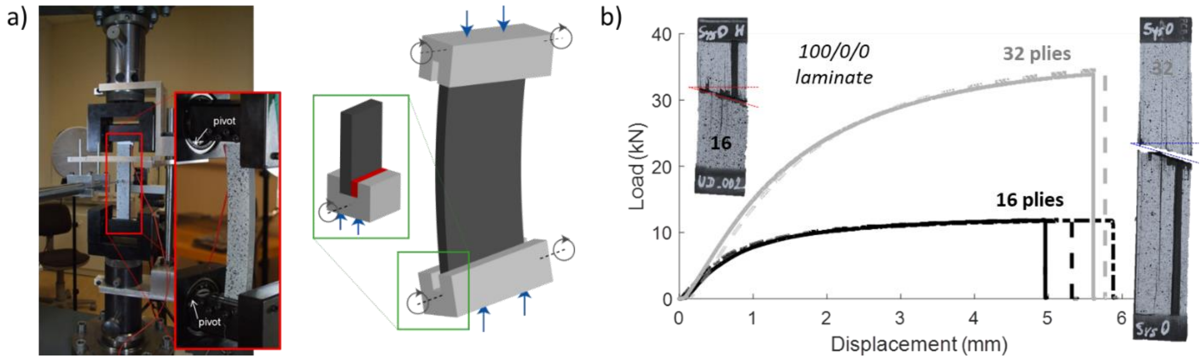

Figure 2 : a) Presentation of the compression with pivots experimental device, b) load/displacement curves for the 0-laminates constituted with 16 and 32 plies

Bending tests on 16-ply and 32-ply 0-laminates have been performed at ONERA. The laminates have been manufactured using the same tooling presented previously and T700GC/M21 material batch as previously. The size of the thin specimens (16 plies) is 130mm x 30mm x 4.2mm and for the thick specimens (32 plies), the size of the specimens is 210mm x 30mm x 8.4mm. Different measurement techniques have been used to improve the understanding of the involved physical mechanisms and to obtain global and local information: (i) LVDT sensor for measuring the evolution of the maximum deflection of the unnotched specimens. The macroscopic curves are highly nonlinear as illustrated in Figure 2b, mainly due to geometrical non-linearity. (ii) Acoustic emission for the detection of damage events during loading. No acoustic event has been detected prior the final failure. Elastic non-linearity (hardening for tension and softening for compression) is also present and explains the evolution of the mid-plane during the loading. (iii) Strain gauges, bonded on the upper and lower faces of the unnotched specimens, for strain measurements, (iv) stereo Digital Image Correlation (performed with the Vic3D system) on the two faces of the specimen with black and white paint speckle for tracking the global displacement, the curvature and to obtain an estimate of the in-plane strains at outer surfaces, as reported in Figure 3. (v) Post-mortem micrographs in order to study the failure pattern of the specimens, as reported in Figure 3. The distribution between the fibre failure in tension and in compression through the thickness can be easily observed on the post mortem pictures, since the grey colours are different for the different failure mechanisms. The evolution of the mid-plane during the tests is also clearly visible. Moreover, an angle is observed for the failure pattern which is about 15°, as illustrated in Figure 2b, which has already been reported in the literature [15]. This multi-instrumentation is an absolute necessity in order to establish the damage and failure scenario for the tested specimens under bending.

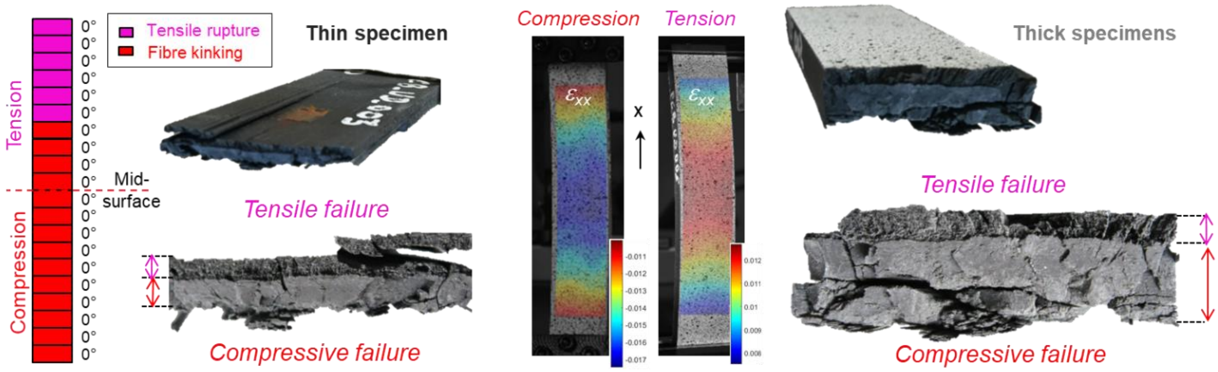

Figure 3 : Load / displacement curves for the 16 and 32 0-plies subjected to bending loading

Therefore, identifying the compressive strength from the test data requires geometrically non-linear finite element analysis to describe the non-linearity. Besides, the longitudinal elastic non-linear behaviour of the Carbon/Epoxy UD plies has to be taken into account ([16,17]), as it is explained in section 3.2. Therefore, difficulties are transferred from experimental analysis to numerical analysis which, all the same, penalises the method for an industrial roll-out.

Specimens	Gauge area mm x mm	Stress at failure MPa (CV %)	Strain at failure % (CV %)
16 plies	130 x 30	-1350 (4.5)	-1.9 (5.2)
32 plies	210 x 30	-1220 (2.8)	-1.7 (2.9)

Table 2: Geometry, stress and strain at failure for the 3 configurations of bending tests on 0-plies

The stress at failure, mentioned in Table 2, corresponds to the longitudinal stress in the lower 0-ply at the experimental failure load. The scattering associated to the tests is about 4% for the thin specimens and 3% for the thick ones, which remains very low compared to pure compression tests.
The value at failure is higher for the thin specimens than for the thick specimens (+10%), meaning the ply thickness has an influence on the strength for bending loading. Moreover, it can be noted that the failure stresses are higher than those obtained for pure compression tests (+51% for thin specimens and +37% for thick specimens). To conclude, the longitudinal compressive strength determined with bending tests are significantly higher than that obtained with pure compression tests, with an associated scattering very low. The failure pattern is relevant and repeatable for all the performed tests. Moreover, the distribution through the thickness of the tension and compression fibre failure modes can be easily observed through the analysis of the post-mortem specimens.

2.3 Innovative tensile test on a specific laminate

In order to be used in aeronautical industries, a proposed alternative test must (i) be easy to perform, (ii) present a low scattering and (iii) its analysis should be as simple as possible for the sake of efficiency in design offices. The only test, which fulfils all these three requirements, is the tensile test. Therefore, one of the key ideas of the present work consists in finding a [$\theta_1/\theta_2/\ldots/90/\ldots/\theta_2/\theta_1$]-laminate that, when

subjected to a tensile loading at the macroscopic scale, fails by fibre compressive failure in the central 90° ply due to the Poisson effect.
Such a kind of laminate failure has already been observed in the literature. For instance, in the framework of the first World Wide Failure Exercise [1], test case number #4 aims at predicting the failure envelope of a $[90/30_2/\text{-}30_2]_s$ Eglass/LY556 laminate in the longitudinal and transverse macroscopic stress plane (Σ_{xx}, Σ_{yy}). The damage scenario for uniaxial loading is the following: Transverse cracks in the 90°-plies appear first, followed by transverse cracks within the -30°-plies. Finally, specimen failure under macroscopic tensile loading is triggered by the fibre compressive failure of the 90°-plies due to the Poisson effect. This test, however, is not suitable for easy identification of the material compressive strength in the fibre direction, since a strong coupling between the ply damage state and its apparent strength in longitudinal compression has been evidenced experimentally [18], which makes accurate identification of X_c more difficult. In order to identify X_c easily using a tensile test on a laminate, it is necessary to find a stacking sequence that is not damaged prior to fibre compressive failure in the 90°-plies.
In order to minimize the required quantity of material, it has been chosen to optimize a symmetrical and balanced 17-ply laminate. The central ply is a 90° oriented ply and is the only 90°-ply in the laminate. The objective of the optimization is to find a laminate whose first damage under tensile loading is fibre failure in compression in the central 90°-ply. Since the ply stacking order does not influence the membrane properties of the laminate, the design space can be described with $[\pm\theta_1/\pm\theta_2/\pm\theta_3/\pm\theta_4/90_{1/2}]_s$ laminates. In the optimization process (4 different ply orientations), the prediction of the behaviour of the laminate up to final failure is performed using the OPFM model detailed in section 3.2. The whole strength analysis method dedicated to laminated plates has been implemented in Matlab©. The computational time on an ordinary laptop computer is about 5 seconds. Among the possible solutions evaluated numerically, the stacking sequence was determined afterwards in order to reduce the risk of premature edge delamination by minimizing the difference in orientation between two consecutive plies. The lay-up considered in the following is $[\text{-}30/\text{-}45/\text{-}30/0_2/30_2/45/90_{1/2}]_s$.
A laminated plate has been manufactured at ONERA using the same tooling and T700GC/M21 material batch as previously. The total thickness of the plate, manufactured with 17 plies, is about 4.45 mm. Five shoulder-end specimens (130 mm x 30 mm gauge) have been machined from the plate. These specimens are numbered from 2 to 6 in the following. Glue has been applied on the edges of the specimens in order to prevent free edge delamination, as reported in Figure 4b.

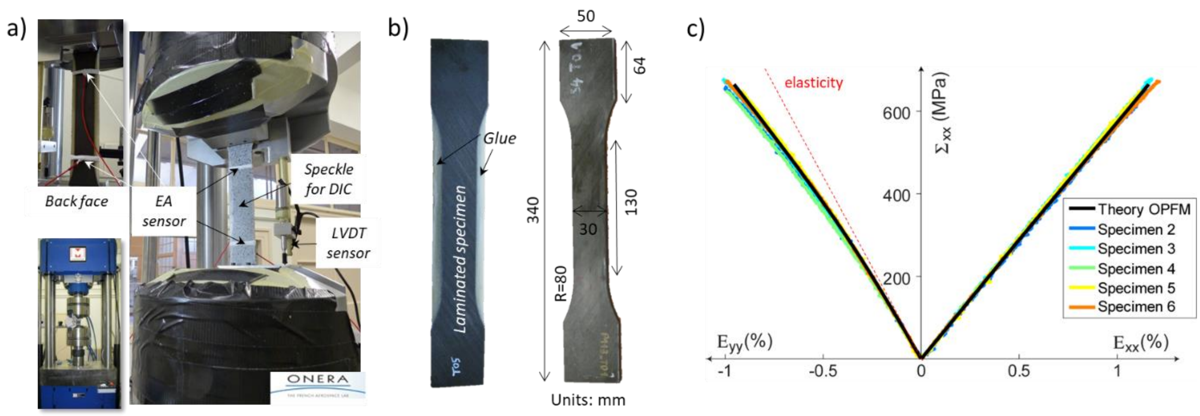

Figure 4 : a) Presentation of the multi-instrumented tensile experimental device, b) of the laminated tested samples, c) of the macroscopic strain (longitudinal and transverse) /stress curves at failure

The tests have been performed in the machine-controlled displacement mode with a 0.2 mm/min constant displacement rate imposed until final failure, illustrated in Figure 4a. It could be noted that for some specimens, tests have been interrupted prior to failure for complementary analyses.

Figure 4c shows that the measured macroscopic stress/strain (longitudinal and transverse) curves are slightly non-linear up to the specimen failure. The macroscopic stress is defined here as the applied load divided by the measured gauge section of the specimens. The longitudinal and transverse strains are measured using the DIC strain fields and a virtual strain gauge located at the centre of the gauge area. The grid size of the virtual strain gauge is 10mm x 10mm and has been determined through a convergence study on the strain at failure.

Failure occurs in the gauge section for all the tested specimens. The post-mortem failure pattern is complex and necessitates additional analysis with other measurement techniques to establish the damage and failure scenario for such a test. No damage event occurs prior to the sudden failure of specimens with glue coated edges. Indeed, no significant acoustic event was recorded prior to the final failure of specimens and no transverse crack could be detected using passive IR thermography. Moreover, thermography images obtained with the IR camera show no transverse crack prior to the final failure and illustrate the suddenness of failure. Specimen 3 has been loaded up to 98 % of the average failure stress of specimens 2, 4 and 5 before interrupting the test. No damage (transverse cracking or edge delamination) could be evidenced using C-scan as well as X-ray computed tomography for two specimens in which the loading has been interrupted prior failure.

Detailed analysis of the post-mortem failure pattern is necessary to validate the expected failure scenario. Thus, X-ray computed tomography, with a 24µm resolution, have been performed at LMPS on specimens 5 and 6 in order to analyse in three dimensions the local failure mechanisms. Figure 5c shows the kink-bands observed in the central 90°-ply in the gauge length of specimen 5. Similar observation was obtained for specimen 6. The kink-bands are observed in the (x,y) plane of the specimen since the Poisson effects generate both compressive transverse and out-of-plane strains. In this plane, the angle formed by the kink-band direction and the fibre direction (y axis) is close to 15° which has already been reported in the literature [15]. Scanning electron microscope (SEM) examinations have been subsequently performed at ONERA to obtain high resolution images of the fibre kinkings, as reported in Figure 5b.

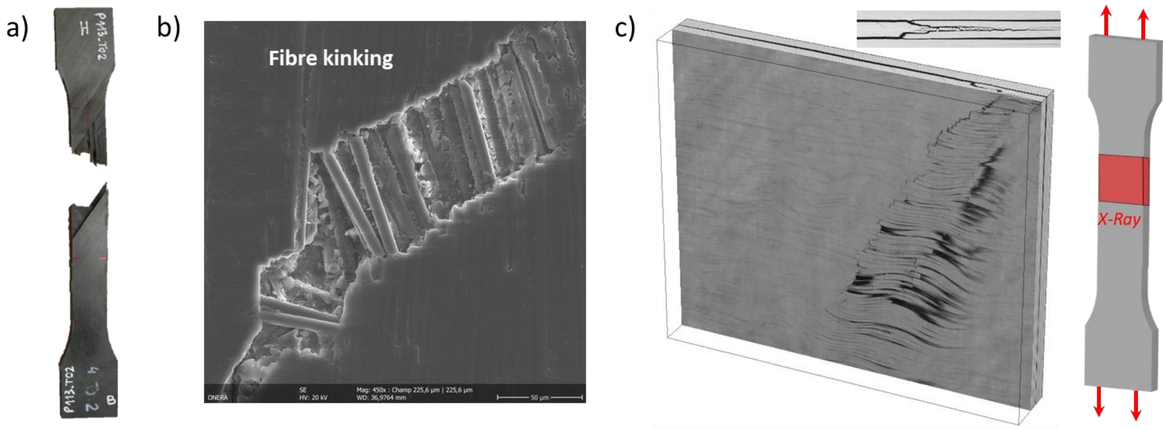

Figure 5 : a) Post-mortem optical analysis of specimen #5, b) SEM analysis of the fiber kinking in the 90-ply c) X-ray tomography images of specimen #5

The average longitudinal compressive strength of specimens 2 to 6 (five specimens with glue coated edges) is X_c=-1034MPa with 2.4% CV. The strain at failure in the fibre compressive failure mode, $X_{\varepsilon c}$, can be directly measured from the test (assuming that no significant edge delamination occurs prior to the final failure) and is equal to the transverse strain in the laminate, as reported in Table 3. The average strain at failure $X_{\varepsilon c}$ is equal to *-1.0%* with 6.2% CV. Compared to classical uniaxial compression tests, the reduction of the scattering of the stress and strain values at failure is explained by the loading mode of the specimen. On the one hand, loading the specimen in tension enables to use long shoulder-end specimens. Thus, local stress concentrations near the machine jaws do not trigger failure, which occurs in the gauge length of the specimen. On the other hand, the compression loading in the 90°-ply is due to the Poisson effect.

Specimens	Gauge area mm x mm	Stress at failure MPa (CV %)	Strain at failure % (CV %)
$[-30/-45/-30/0_2/30_2/45/90_{1/2}]_s$	130 x 30	-1034 (2.4)	-1.0 (6.2)

Table 3: Geometry, stress and strain at failure for tensile tests on a specific laminate

2.4 Conclusions on test results

The longitudinal compressive strength identified using the tensile test has been compared with values identified on conventional compression tests performed at ONERA using the same material batch, but also with bending tests on 0-ply with two different thicknesses, as reported in Figure 6. The strengths, identified at the ply scale by inverse method, obtained with bending tests are higher and seem dependent on the ply thickness. Therefore, the choice of the scale of modelling to study the fibre kinking is a key and should allow demonstrating that test results are consistent (but not those due to premature failure).

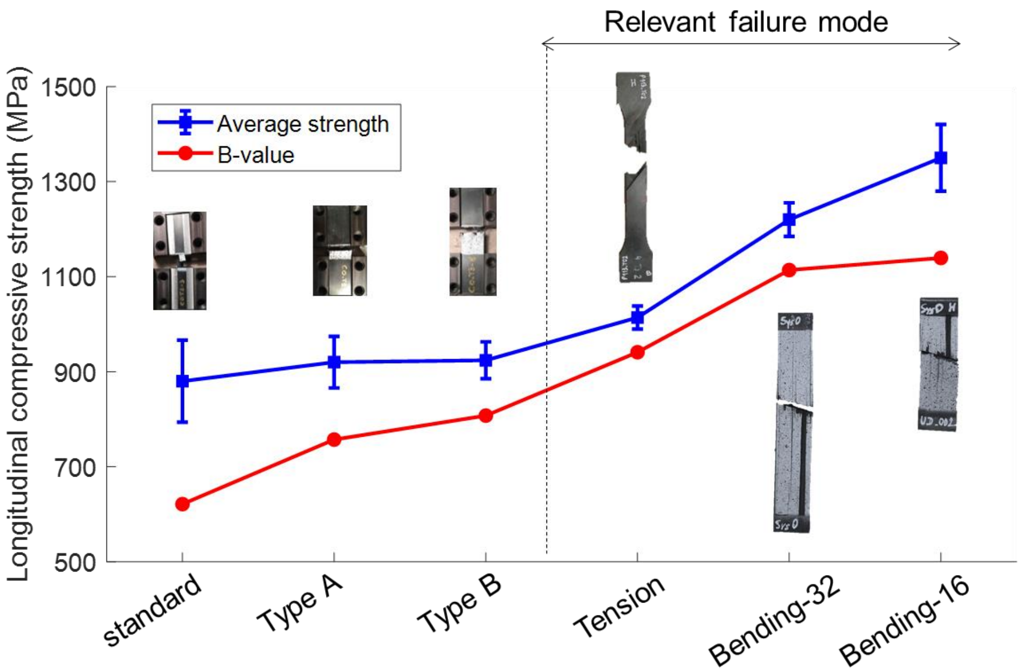

Figure 6 : Comparison between the longitudinal compressive strengths identified using compression tests, tension test and bending tests.

3 MODELLING STRATEGY TO ANALYSE AVAILABLE TESTS

3.1 Micromechanical model to predict the longitudinal compressive strength of a UD ply

A model defined at the micromechanical scale has been proposed by Grandidier [11,19]. This model is based on finite element simulations with enhanced elements to capture the fibre buckling embedded within the matrix. Based on this work, a simplified analytical model has been proposed by Grandidier [20] later in order to be used in design office to determine the longitudinal compressive strength, considering compressive loadings or bendings. The model accounting for the combined contributions of fibre micro-buckling [21] and the structural effect (stacking sequence, strain gradient) [22–24] was proposed to describe the mechanism of failure in compression under flexural loading [20]. This model is also analytical so that it can be used for the fast design loop of composite structures.

First models for local instability, to predict the contributions of fibre micro-buckling, appear in the 1960s. Rosen [25] estimated the instability elastic stress as being the shear modulus of the ply. However,

the elastic buckling assumption for failure explanation was quickly reconsidered. Matrix plasticity appeared to be an impacting and strong governing parameter for fibre instability mechanism development. Furthermore, and as for any mechanism of instability, geometric defects have to be considered and, for compression load in fibre direction, fibre misalignment defects are the main impacting parameter. This variability of long fibre composite materials was therefore included into the models. The local failure mechanism accepted by the scientific community puts together a sequence of phenomena: under compression load a little fibre misalignment triggers fibre buckling, the matrix provides the assembly of the fibres but evolves to plasticity which amplifies therefore the instability, fibre failure appears successively by developing a kink band [21]. The main governing parameters of this mechanism are the nonlinearity of matrix properties and fibres initial undulation defects ϕ_0.
The most efficient models existing in the literature account quite well for these effects. Budiansky and Fleck [21] modelled the non-linear shear behaviour of UD (shear strain) vs. (shear stress) by using a Ramberg-Osgood (RO) description, reported in Eq. 1:

$$\frac{\gamma}{\gamma_{UD}^{y}} = \frac{\tau}{\tau_{UD}^{y}} + \frac{3}{7}\left(\frac{\tau}{\tau_{UD}^{y}}\right)^{n_{UD}} \tag{1}$$

It involves three material parameters ($\tau_{UD}^{y}, G_{UD}, n_{UD}$) or ($\gamma_{UD}^{y}, \tau_{UD}^{y}, n_{UD}$). G_{UD} is the in-plane shear modulus of the composite, τ_{UD}^{y} is a nominal shear yield stress for which the secant modulus is reduced to 70% of its initial value G_{UD}. γ_{UD}^{y} is defined as the elastic strain at the shear stress τ_{UD}^{y} so that $\tau_{UD}^{y}= G_{UD}\ .\ \gamma_{UD}^{y}$. The coefficient 3/7 is specific to a choice made in [21] related to the definition of τ_{UD}^{y}. The compressive strength, referred to as σ_{UD}^{stab}, and calculated using Budiansky and Fleck's model, is defined as the maximum stress applied on UD before the fibre instability, as reported in Eq. 2.

$$\sigma_{UD}^{stab} = \frac{1}{1 + n_{UD}\ \left(\frac{3}{7}\right)^{\frac{1}{n_{UD}}} \left(\frac{\phi_0/\gamma_{UD}^{y}}{n_{UD} - 1}\right)^{\frac{n_{UD}-1}{n_{UD}}}} \tag{2}$$

The structural effect results in the increase of UD failure compressive strain and stress with respect to σ_{UD}^{stab}. It is due to several mechanisms that do not take place at the UD mesoscopic scale but rather at a larger, macroscopic scale (laminate). Three factors are included in the structural effect, namely the deformation gradient through the thickness due to bending loadings, the thickness of UD and the stiffness of off-axis neighbouring plies. Experimental observations on the structural effect have been experimentally detailed and compared by Grandidier [20], ending with the proposal of an analytical model (reported in Eq. 3) to predict the stress due to structural application.

$$\sigma_{UD}^{struct} = 2r_{gf}\,\frac{\pi}{e_b}\sqrt{\frac{E_m E_f}{1-\nu_m^2}V_f(1-V_f)} \tag{3}$$

where r_{gf} is the gyration radius of fibre r_{gf}= *I/S* , with *I* the second moment of area of the fibre, and *S* the area of the fibre's cross section (it is equivalent to the fibre diameter divided by 4, in case of fibres are considered circular), E_m and ν_m are respectively the Young's modulus and the Poisson's ratio of the matrix, E_f the longitudinal elastic modulus of the fibre, V_f the volume fraction of fibres and e_b the characteristic thickness of UD involved in the instability mode (a fraction of the total thickness of UD), which is discussed below.
Let us start with the definition of the critical thickness, e_c where the ply thickness is noted e. As an example, for a UD layer subjected to bending, only the part in compression is considered for critical thickness (e_c). For a monolithic UD stacking (only 0° plies), the instability mode is located near the free edge due to the deformation gradient. As it has been demonstrated by Drapier [26], the modal shape of the plastic instability has an impact on critical values. In the case of UDs under bending only a reduced part of thickness is considered to contribute to compression failure due to the distribution of the strain. In order to easily approximate this effect, Grandidier [20] proposed the characteristic thickness to be $e_b = 0.4\ e_c$ which permits correlation with experimental results in similar configurations (see [20] for details). For a laminate with different ply orientations, in case of 0-plies are located near the edge, these

latter plies bear a high compression stress with a reduced gradient due to their low thickness. Consequently, the modal shape of instability extends on all UDs thickness, and the characteristic thickness should be approximated by e_b=e_c as proposed in [20]. In case of a laminate where 0-plies are located at mid-plane, these latter plies bear only the compression part applied on half of the ply thickness, and the characteristic thickness should be approximated by $e_b = e_c = 0.5\ e$ as proposed in [20].

Finally, the proposed model considers both the micro-buckling mechanism (σ_{UD}^{stab}) and the structural effect (σ_{UD}^{struct}). The estimated compressive strength is called critical, referred to as σ_{UD}^{crit}, is higher than σ_{UD}^{stab}, since it is defined in Eq. 4:

$$\sigma_{UD}^{crit} = \sigma_{UD}^{stab} + \sigma_{UD}^{struct} \tag{4}$$

3.2 Mesoscopic Progressive Failure Model

The Onera Progressive failure approach (OPFM), developed at Onera since many years for composite materials with thermoset matrix [9], has been considered. The behaviour of the T700/M21 material up to failure should be modelled considering the different sources of non-linearity (thermal residual stresses, viscosity, elastic non-linearity, intra-ply damage) at the ply scale using a laminate theory extended to non-linear behaviour. The prediction of the local non-linear mesoscopic behaviour up to the specimen failure is performed with OPFM, which is briefly summarized in this section. The present multiscale failure approach considers the unidirectional (UD) ply as the elementary entity of modelling and is predictive for different stacking sequences. It could be decomposed into four main steps.

Firstly, in order to predict accurately the failure of a ply in a laminate, it is necessary to estimate correctly the mesoscopic stresses and strains. A non-linear thermo-viscoelastic behaviour has been proposed in Eq. 5.

$$\underline{\sigma} = \underline{\underline{\tilde{C}}}:\left(\underline{\epsilon} - \underline{\epsilon}^{th} - \underline{\epsilon}^{ve} - \underline{\epsilon}^{nl}\right) \tag{5}$$

where $\underline{\sigma}$ is the mesoscopic stress, $\underline{\underline{\tilde{C}}}$ the effective rigidity, $\underline{\epsilon}$ the total strain, $\underline{\epsilon}^{th}$ the thermal strain (in order to take into account the thermal residual stresses, which are essential to predict accurately the first ply failure), $\underline{\epsilon}^{nl}$ the non-linear elastic strain (in order to describe the hardening observed experimentally on UD plies subjected to longitudinal tensile loadings and especially on new generations of composite materials such as T700GC/M21 [16] or observed on the studied material), and $\underline{\epsilon}^{ve}$ the viscous strain.

Secondly, the prediction of the ply failure within the laminate is performed with a failure criterion, based on Hashin's hypotheses [27], distinguishing the fibre failure mode and the in-plane interfiber failure mode and modelling separately the failure mechanisms in tension and in compression for each failure mode. The main improvement of the fibre failure criterion, as compared to Hashin's criterion is to consider the influence of the in-plane shear on the ply failure in compression. The main improvement of the interfiber failure criterion is a better description of the reinforcement of the apparent strength of the material for combined in-plane shear and transverse compressive loadings.

Thirdly, when a ply within the laminate is broken in interfiber mode (*i.e.* when transverse cracks are present in the ply), its mechanical properties are progressively degraded using a thermodynamical degradation approach based on damage modelling already developed at Onera.

Fourthly, for a laminated unnotched coupon, the final rupture could be due to the first ply failure in fibre mode or in transverse compression. It is important to note that the longitudinal compressive strength, defined at the ply scale, has been updated considering the micromechanical approach, described in section 3.1, depending on the ply thickness and the applied loading.

3.3 Estimation of the apparent longitudinal compressive strengths at ply scale

The micromechanical model proposed by Grandidier has been fully identified on the T700GC/M21 material. In order to use the present model, several experimental data are required.

Firstly, analysis of the microstructure allows to measure the parameters related to the structural effect, such as the volume fraction of fibres and the radius of these fibres, is performed. In order to perform that, CT-scans performed on a T700/M21 cross-ply laminate has been analysed. Figure 7a presents a side of CT-Scan performed at the University of Southampton with a resolution of 0.69µm on a T700/M21 cross-ply laminate (only the 0° ply is analysed). The distribution of the fibre radius is also reported and the average value of the Weibull distribution is r_f=3.25µm and the volume fibre ratio of the material is equal to V_f=56%. In a previous study [28], the mechanical properties of fibres and matrix have been determined considering an inverse method using a Mori-Tanaka method in order to obtain the relevant mechanical properties measured at the ply scale considering tensile tests on 0-plies, 90-plies and $[\pm 45]_s$ laminates. Then, the plasticity of the matrix, which is approximated with a Ramberg-Osgood law, necessitates the identification of three parameters (τ_{UD}^{y}, G_{UD}, n_{UD}). These parameters can be determined by inverse identification considering a tensile test on a $[\pm 45]_s$ laminate, as reported in Figure 7b. Finally, the last parameter to identify is the initial misalignment of the fibres, which will generate the fibre kinking into the composite material. This value has been determined by inverse identification considering the tensile test on a specific laminate which failed in compression. The identified value is equal to $\phi_0 = 2°$ which is consistent with data found in literature [20,29] and the identified strength for the UD ply subjected to compressive loading is equal to X_c = -1056 MPa compared to the experimental one X_c = -1034MPa, an error of 2.1% is obtained.

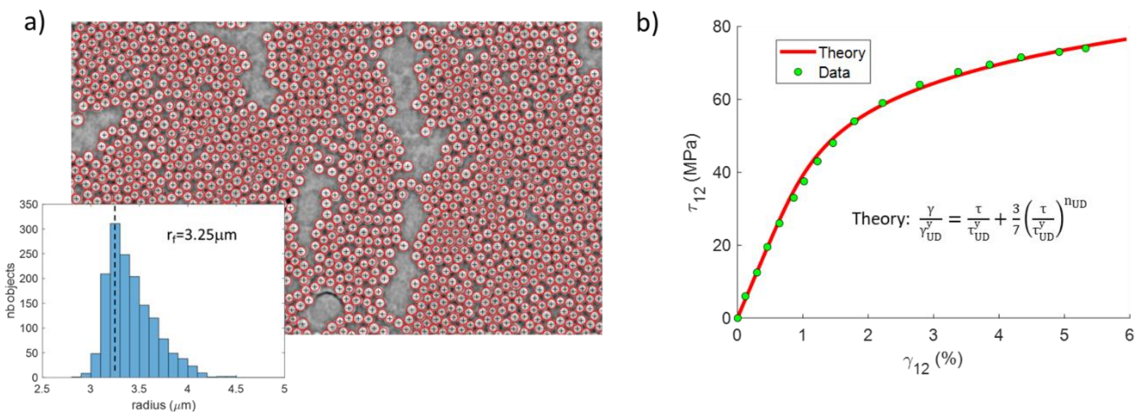

Figure 7 : Identification of different parameters of the micromechanical approach a) considering the microstructure of T700/M21 UD ply and b) a tensile test on $[\pm 45]_s$ laminate

Then, it becomes possible to predict the longitudinal compressive stress at failure for the two bending tests presented in section 2.2. Figure 8 presents the comparisons between the predicted and measured longitudinal stress at failure for the lower 0-ply in the two specimens, constituted with respectively 16 and 32 0-plies, subjected to bending loading. Firstly, the model accurately captures the evolution of the strength for compression or for bending loadings, as it predicts an increase of the strength for bending loadings. Moreover, the decrease of the strength as a function of the total thickness of the laminate is also well predicted. Secondly, the error between the predictions and the test data are in good agreement with experimental data (lower than 10%). Those first results are encouraging for the use of a model at microscale which allows demonstrating that the compressive tests and bending tests are consistent if they are analysed at the relevant scale, taking into structural effects. It can be noted that the tests performed on pure 0-ply subjected to compression present a lower strength than the other tests (tension and bending) due to premature failure in the jaws and are not consistent with the model prediction. The longitudinal compressive strength defined at the ply scale can be determined with the proposed micromechanical model and can be used then in a multiscale approach to predict the failure of laminates with different stacking sequences subjected to different types of loading.

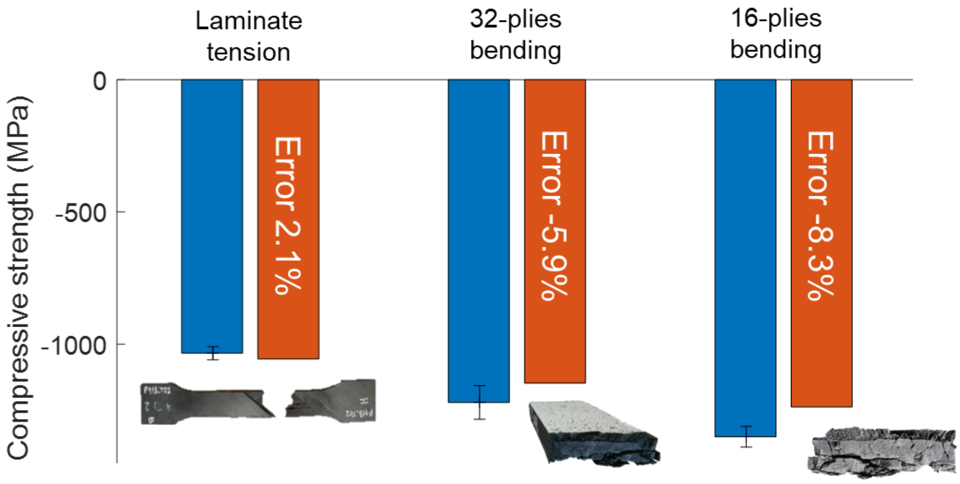

Figure 8 : Comparison between the experimental and predicted compressive strengths obtained with the micromechanical model.

4 CONCLUSIONS

The present study has proposed a critical analysis of the available existing tests in order to determine the longitudinal compressive strength of a UD ply. The (i) standardized compressive tests on UD-ply, the (ii) alternative tensile test on a specific lay-up proposed by ONERA and (iii) additional bending tests on UD-ply have been considered. The measured compressive strength at the ply scale is different for those tests and the highest strength value is obtained for bending loadings. In order to analyze such tests (compression, tension and bending), a micromechanical model has been considered and allows demonstrating that the variation of the longitudinal compressive strength obtained at the UD ply scale for tension and bending tests are consistent if fiber kinking is considered at microscale scale, which seems to be the relevant scale of analysis. This micromechanical model has been used to identify the strength at the ply scale of the Onera Progressive Failure Model, which has been used to predict successfully the failure of different laminates subjected to compressive loadings.

REFERENCES

[1] P.D. Soden, M.J. Hinton, A.S. Kaddour, A comparison of the predictive capabilities of current failure theories for composite laminates, Compos. Sci. Technol. 58 (1998) 1225–1254.

[2] MIL-HDBK-17-1F: Composite Materials Handbook, Volume 1 - Polymer Matrix Composites Guidelines for Characterization of Structural Materials, U.S. Department of Defense, 2002.

[3] J. Lee, C. Soutis, Thickness effect on the compressive strength of T800/924C carbon fibre-epoxy laminates, Compos. Part Appl. Sci. Manuf. Inc. Compos. Compos. Manuf. 36 (2005) 227.

[4] J. Lee, C. Soutis, A study on the compressive strength of thick carbon fibre-epoxy laminates, Compos. Sci. Technol. 67 (2007) 2015–2026.

[5] AECMA standard EN-2850, Aerospace series carbon fibre thermosetting resin unidirectional laminates. Compression test parallel to fibre direction, 1997.

[6] N. Carbajal, F. Mujika, Determination of compressive strength of unidirectional composites by three-point bending tests, Polym. Test. 28 (2009) 150–156.

[7] N. Carbajal, F. Mujika, Determination of longitudinal compressive strength of long fiber composites by three-point bending of $[0_m/90_n/0_p]$ cross-ply laminated strips, Polym. Test. 28 (2009) 618–626.

[8] P.J. Callus, The effects of hole-size and environment on the mechanical behaviour of a quasi-isotropic AS4/3501-6 laminate in tension, compression and bending, Defense Science and Technology Organisation of Australian Government, 2007.

[9] F. Laurin, C. Julien, P. Paulmier, Damage and strength analysis of open-hole laminated plates under tensile, compressive and bending loadings, in: 2016: pp. 1–8.

[10] M.R. Wisnom, On the Increase in Fracture Energy with Thickness in Delamination of Unidirectional Glass Fibre-Epoxy with Cut Central Plies, J. Reinf. Plast. Compos. 11 (1992) 909.
[11] J.-C. Grandidier, G. Ferron, M. Potier-Ferry, Microbuckling and strength in long-fiber composites: theory and experiments, Int. J. Solids Struct. 29 (1992) 1753–1761.
[12] O. Allix, P. Ladeveze, E. Vittecoq, Modelling and identification of the mechanical behaviour of composite laminates in compression, Compos. Sci. Technol. 51 (1994) 35–42.
[13] M.R. Wisnom, T. Reynolds, N. Gwilliam, Reduction in interlaminar shear strength by discrete and distributed voids, Compos. Sci. Technol. 56 (1996) 101.
[14] C. Hochard, J. Payan, O. Montagnier, Design and computation of laminated composite structures, Compos. Sci. Technol. 65 (2005) 474.
[15] T.J. Vogler, S.-Y. Hsu, S. Kyriakides, On the initiation and growth of kink bands in fiber composites. Part II: analysis, Int. J. Solids Struct. 38 (2001) 2653–2682.
[16] C. Huchette, Analyse multiéchelle des interactions entre fissurations intra et inter laminaire dans les matériaux composites stratifiés, Doctorate thesis of Université de Paris VI, 2005.
[17] T. Ishikawa, M. Matsushima, Y. Hayashi, Hardening non linear behaviour in longitudinal tension of unidirectional carbon composites, J. Mater. Sci. 20 (1985) 4075–4083.
[18] G. Eyer, O. Montagnier, C. Hochard, J.-P. Charles, Effect of matrix damage on compressive strength in the fiber direction for laminated composites, Compos. Part A. 94 (2017) 86–92.
[19] S. Drapier, J.-C. Grandidier, M. Potier-Ferry, Towards a numerical model of the compressive strength for long fibre composites, Eur. J. Mech. - ASolids. 18 (1999) 69–92.
[20] J.-C. Grandidier, P. Casari, C. Jochum, A fibre direction compressive failure criterion for long fibre laminates at ply scale, including stacking sequence and laminate thickness effects, Compos. Struct. 94 (2012) 3799–3806.
[21] B. Budiansky, N.A. Fleck, Compressive failure of fibre composites, J. Mech. Phys. Solids. 41 (1993) 183–211.
[22] S. Drapier, C. Gardin, J.-C. Grandidier, M. Potier-Ferry, Structure effect and microbuckling, 9th Fr. Natl. Colloq. Compos. Mater. 56 (1996) 861–867.
[23] C. Gardin, J.C. Grandidier, M. Potier-Ferry, Homogenized models for the modelling of instability in long fibre media, Rev. Mec. Appliquée Théorique. 1 (2002) 171–203.
[24] M.R. Wisnom, J.W. Atkinson, Constrained buckling tests show increasing compressive strain to failure with increasing strain gradient, Compos. Part A. 28 (1997) 964.
[25] B.W. Rosen, Mechanics of composite strengthening, 1965.
[26] S. Drapier, J.-C. Grandidier, M. Potier-Ferry, A structural approach of plastic microbuckling in long fibre composites: comparison with theoretical and experimental results, Int. J. Solids Struct. 38 (2001) 3877–3904.
[27] Z. Hashin, Failure criteria for unidirectional fiber composites, J. Appl. Mech. 47 (1980) 329–334.
[28] F. Laurin, N. Carrere, J.-F. Maire, Effect of diffuse porosity on mechanical properties, RT 10/11905 DMSC, 2009.
[29] P.-Y. Mechin, V. Keryvin, J.-C. Grandidier, D. Glehen, An experimental protocol to measure the parameters affecting the compressive strength of CFRP with a fibre micro-buckling failure criterion, Compos. Struct. 211 (2019) 154–162.